F-doped carbon/Co_3O_4 composite catalyst for alkaline oxygen evolution

Mengjie Gao[#], Zhaodi Wang[#], Weiruo Liu and Yunpu Zhai*

College of Chemistry, Zhengzhou University, 100 Kexue Avenue, Zhengzhou 450001, Henan, PR China

[#]These authors contributed equally to this work.

* Corresponding author. E-mail address: yunpu.zhai@zzu.edu.cn (Y. Zhai).

Abstract

Electrocatalytic water splitting is a sustainable way to produce hydrogen energy. However, the oxygen evolution reaction (OER) at the anode always has sluggish kinetics and low energy conversion efficiency, which is the major bottleneck for water splitting. In this paper, the electronic structure of the Co_3O_4/carbon composites was regulated by anion doping. The F-doped carbon substrate is compounded with ZIF-67, and the active component Co_3O_4 is encapsulated in the skeleton formed by ZIF-67. The prepared hybrid nanocomposite catalyst F-Co_3O_4@NF has excellent OER performance. It requires an overpotential of only 172 mV with the current density of 50 mA cm^{-2}, and the Tafel slope is 88 mV dec^{-1}. It can maintain good stability after 24 hours of continuous operation, and the catalytic activity exceeds most of the similar series of catalysts. The characterization show that F doping can affect the catalytic activity in the form of adjusting the electronic structure and lifting *d* band center. These structural changes effectively optimize the adsorption/desorption capacity of the composite catalyst for hydrogen and oxygen intermediates in the catalytic process, thereby improving the catalytic activity for alkaline oxygen evolution.

Key words: Co_3O_4, electrocatalysts, halogen-doped, carbon, oxygen evolution reaction

1 Introduction

The oxygen evolution reaction (OER) is of critical importance as the key reaction in electrocatalytic water splitting devices and rechargeable metal-air batteries.[1] Nevertheless, the multistep proton-coupled electron transfer processes involved in OER lead to the sluggish kinetics, which severely constrains the energy conversion efficiency. At present, the most efficient electrocatalysts for OER are yttrium oxide and ruthenium oxide[2, 3], but their scarcity and high prices limit their mass production and wide application.

Earth-abundant transition metals, in particular Co_3O_4 which has low price and mixed-valence cobalt (II, III), have recently been considered as one of the promising alternatives to noble metal oxides for efficient OER in alkaline electrolytes[4-6]. However, the activity of Co_3O_4 is still far less than that of noble metal oxides. Recently, it is reported that the intrinsic activity of electrocatalysts can be enhanced by tuning their electronic states through nonmetal doping.[7] For example, Wu et al. demonstrated a modulation of the electron densities of the catalytic sites of $NiCo_2S_4$ nanowire arrays (NWs) for high performance hydrogen evolution reaction (HER) activity by using nitrogen as the modulator.[7] They prepared nitrogen-doped $NiCo_2S_4$ nanowire arrays by replacing part of the catalytic sulfur sites with N. The electron densities of the sulfur sites were decreased due to the strong interaction between metal and nitrogen. Therefore, the H–S interaction was weakened, which facilitate the H* desorption from the remaining sulfur sites to form H_2 in the HER. The catalyst showed excellent HER performance in water splitting (1 M KOH electrolyte) with an overpotential of only 38 mV at 10 mA cm^{-2}. Kou's group constructed a composite catalyst of nitrogen-doped Ni_3S_2 nanosheets[8], which showed an overpotential of 155 mV at 10 mA cm^{-2} in HER reaction. Theoretical calculations show that the excellent catalytic activity of nitrogen-doped Ni_3S_2 is due to the enrichment of active sites with good H adsorption capacity. Xin et al[9] reported self-supporting Ni_3S_2 nanosheet arrays doped with F ions (F-Ni_3S_2/NF). In 1 M KOH electrolyte, it showed excellent HER performance with an overpotential of only 38 mV at current density of 10 mA cm^{-2}. Theoretical calculations

revealed that the incorporation of F atoms into the Ni_3S_2 lattice causes strong electronic coupling between metal cations and non-metallic anions, thereby shifting the d-band up, which is not only beneficial to increase the adsorption energy of intermediate hydrogen on the catalyst surface, but also accelerates the dissociation of water molecules on the catalyst surface. They have proved that the adjustment of the electron density of the active metal by the anion is the reason for the improvement of the water electrolysis performance. Doping anions with strong electronegativity into the active component can adjust the electron density and improve the adsorption effect, thereby improving the electrocatalytic activity.

Metal-organic framework materials[10] have attracted much attention due to their diversity of composition and structure. They can be used in the field of sensors[11, 12], electrocatalytic oxygen reduction[13, 14], electrocatalytic water splitting[15-20] and so on. The two-dimensional Zeolitic Imidazolate Framework (ZIF) materials have ultra-thin porous layers and very large surface area[21, 22], which promote the exposure of active sites and the diffusion of protons/electrons[23, 24]. The unique pore structure is also suitable for gas adsorption and capillary effect to increase its wettability[1, 17]. These characteristics make the two-dimensional ZIF material more efficient for OER in electrolysis of water[25, 26]. Using two-dimensional ZIF-67 as the precursor of Co_3O_4 can not only reduce the agglomeration of active sites，but also provide a large surface area with exposing abundant active sites.

It is noted that F has the strongest electronegativity, we reasonably speculate that the addition of F to Co_3O_4 may produce a more suitable electronic structure, thereby improving the electrocatalytic activity of Co_3O_4 for OER. Here, we reported F-doped carbon/Co_3O_4 composites grown on the nickel foam. The catalyst structure can be adjusted by changing the halogen type, thereby affecting the catalytic performance. The synthesized F-doped carbon/Co_3O_4@NF catalyst provides abundant active sites. Additionally, F doping causes a decrease in the local electron density of Co_3O_4, regulates the electronic structure of the catalyst, and increases the adsorption capacity of the catalyst surface to the intermediates, thereby obtaining excellent OER catalytic performance for water electrolysis. It requires an overpotential of only 172 mV at a

current density of 50 mA cm^{-2}. After 24 hours of continuous operation at constant voltage, the current density is maintained at about 94%, which proves the high stability of the material.

2 Results and Discussion

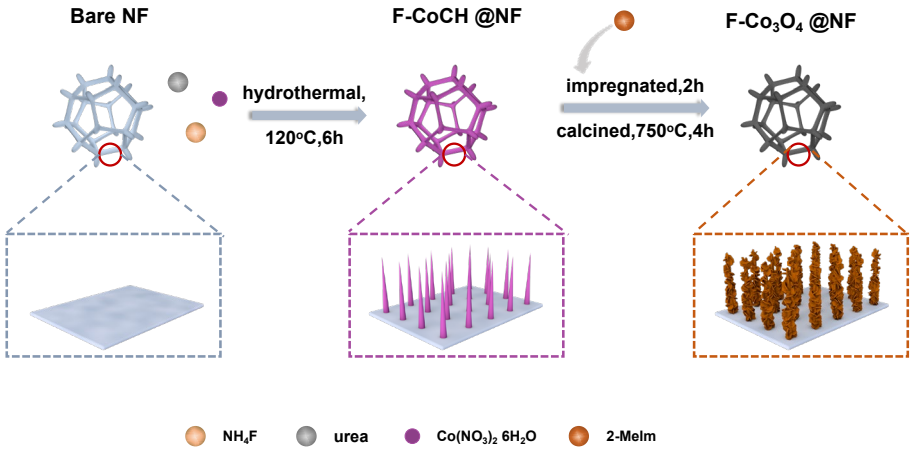

Scheme1. Roadmap for the synthesis of F-Co_3O_4/carbon@NF composite catalysts

The synthesis process of F-Co_3O_4@NF is shown in Scheme 1 (for details of synthesis, see Supporting Information). In the first step, $Co(NO_3)_2{\cdot}6H_2O$, CH_4N_2O and NH_4F were dissolved in deionized water to form a purple clear solution, which was put into the reactor with the cleaned nickel foam (NF). After hydrothermal treatment at 120 °C for 6 h, a light purple F-doped needle-like nanoarray substrate (F-CoCH@NF) was formed on the surface of nickel foam. CoCH was obtained through the reaction of cobalt ions with hydroxide and carbonate in the solution formed by the thermal decomposition of urea. In addition, the mixture of urea and NH_4F can produce special morphology due to thermodynamic preference during the hydrothermal process[3, 27, 28], which provides a large surface area for the subsequent formation of ZIF-67. In the second step, F-CoCH@NF was immersed in 2-methylimidazole solution to form a ZIF-67 structure with Co atom as the center and 2-methylimidazole as the ligand. The ZIF-67 was firmly embedded on the surface of the needle-like carbon substrate. The possible growth mechanism of ZIF-67 is that the H^+ released by 2-methylimidazole has an etching effect on the cobalt compound on the surface of CoCH@NF, resulting in the

release of Co^{2+} to coordinate with 2-methylimidazole for in-situ growth of ZIF-67 nanocrystals. Subsequently, the sample was pyrolyzed in flowing Ar gas at 750°C, and the ZIF-67 structure was changed to nano-sized Co_3O_4 highly dispersed on F-doped carbon-based arrays, while the dodecahedron organic ligand structure was converted to two-dimensional porous carbon nanosheets (orange flake hexagon in Scheme1).

2.1 Structural of composites

The SEM image (Fig. S1a) demonstrates the in-situ growth of needle-like F-CoCH on foam nickel with uniform size. The TEM images (Fig. S1b, c) reveal the good internal crystallinity of the needle-like F-CoCH, with defects detected only at the edges. HRTEM image reveals clear and abundant lattice fringes (Fig S1d), with a lattice spacing of 0.50 nm, corresponding to the (020) crystal plane of CoCH (JCDPS No.48-0083). The uniform distribution of C, N, Co, and F elements (Fig S1e-h) proves the successful incorporation of F element into CoCH.

After reacting with 2-methylimidazole and calcination, F-CoCH was converted to F-Co_3O_4 and the organic component was carbonized. The needle-like arrays were transformed to two-dimensional hexagonal nanosheets (Fig. 1a). The TEM image (Fig. 1b) reveals well-distributed black dots on the hexagonal nanosheets. These black dots correspond to Co_3O_4, while the lighter black areas represent carbon that is a result of the carbonization of 2-methylimidazole. The HRTEM image of F-Co_3O_4/carbon@NF (Fig. 1c) depicts a large area of ordered lattice fringes with a lattice spacing of about 0.28 nm, in agreement with the (220) crystal plane of Co_3O_4 (spinel phase with Fd-3m structure). The selected area electron diffraction (Fig. 1d) shows five diffraction rings that correspond to the (111), (311), (440), (620), and (751) crystal planes of Co_3O_4, indicating a highly crystalline material. The element distribution maps of F-Co_3O_4/carbon@NF (Fig. 1e-i) demonstrate that the O and Co elements are evenly distributed on the hexagonal structure, while the content of N and F is low but predominantly present on the hexagonal structure.

In order to study the phase structure of the catalyst, we used X-ray diffraction (XRD) to analyze the phase and composition of the intermediates during the synthesis of F-Co_3O_4 @ NF. The curves in the Figure1e are the XRD spectra of F-CoCH@NF

and F-Co_3O_4 @ NF, respectively. The XRD pattern of F-CoCH @ NF shows that the diffraction peak signal of the composite obtained by hydrothermal method corresponds to the standard value of CoCH (JCDPS No.48-0083), indicating that Co is dispersed on the carbon substrate in the form of compound CoCH during the hydrothermal process. The diffraction peak of the F-Co_3O_4 @ NF composite material obtained by calcining the CoCH@NF after impregnation corresponds to the standard value of Co_3O_4 (spinel phase with Fd-3m structure) (JCDPS No.09-0418), corresponding to (111), (220), (311), (222), (400), (511), (440) crystal planes at 18.9º, 31.2º, 36.8º, 38.5º, 44.8º, 59.3º, 65º, respectively. Raman and X-ray photoelectron spectroscopy (XPS) spectra corroborate the copresence of Co^{2+} and Co^{3+} ions (Figure S3, Supporting Information). It is worth noting that compared with F-CoCH@NF, the diffraction peak of CoCH in the XRD pattern of F-Co_3O_4@NF almost completely disappeared, indicating the transformation of CoCH to Co_3O_4.

In order to investigate the impact of halogens on catalysts, we also prepared two sets of samples: bare ones without halogen, namely CoCH@NF and Co_3O_4/C@NF, and Cl-doped ones, namely Cl-CoCH@NF and Cl-Co_3O_4/C@NF. The preparation process for these samples was similar to that of F-Co3O4/C@NF. SEM images of both CoCH@NF and Cl-CoCH@NF show needle-like arrays, as depicted in Figure 2a and b. However, in the sample without halogen (CoCH@NF), the needle-like arrays are adhered to each other, exhibiting the morphology of nanoflowers. Moreover, the needle-like morphology of the sample doped with Cl (Cl-CoCH@NF) is sparser than that of the sample with F doping. Figure 2d, e, f is the morphology of Co_3O_4@NF samples with different halogens. It can be seen that large number of hexagonal two-dimensional nanosheets are evenly covered on the carbon substrate. The surface of these hexagonal nanosheets is rough and the side length is about 300 nm. These could be that the two-dimensional ZIF-67 grows on the surface of the needle-like carbon-based array and carbonizes after high-temperature calcination, causing the collapse of the structure and forming a rough surface. Combined with the results of XRD, the Co atom in the center of ZIF-67 is transformed into the active site Co_3O_4, and the framework structure around Co_3O_4 maintains a two-dimensional hexagonal nanosheet

structure.

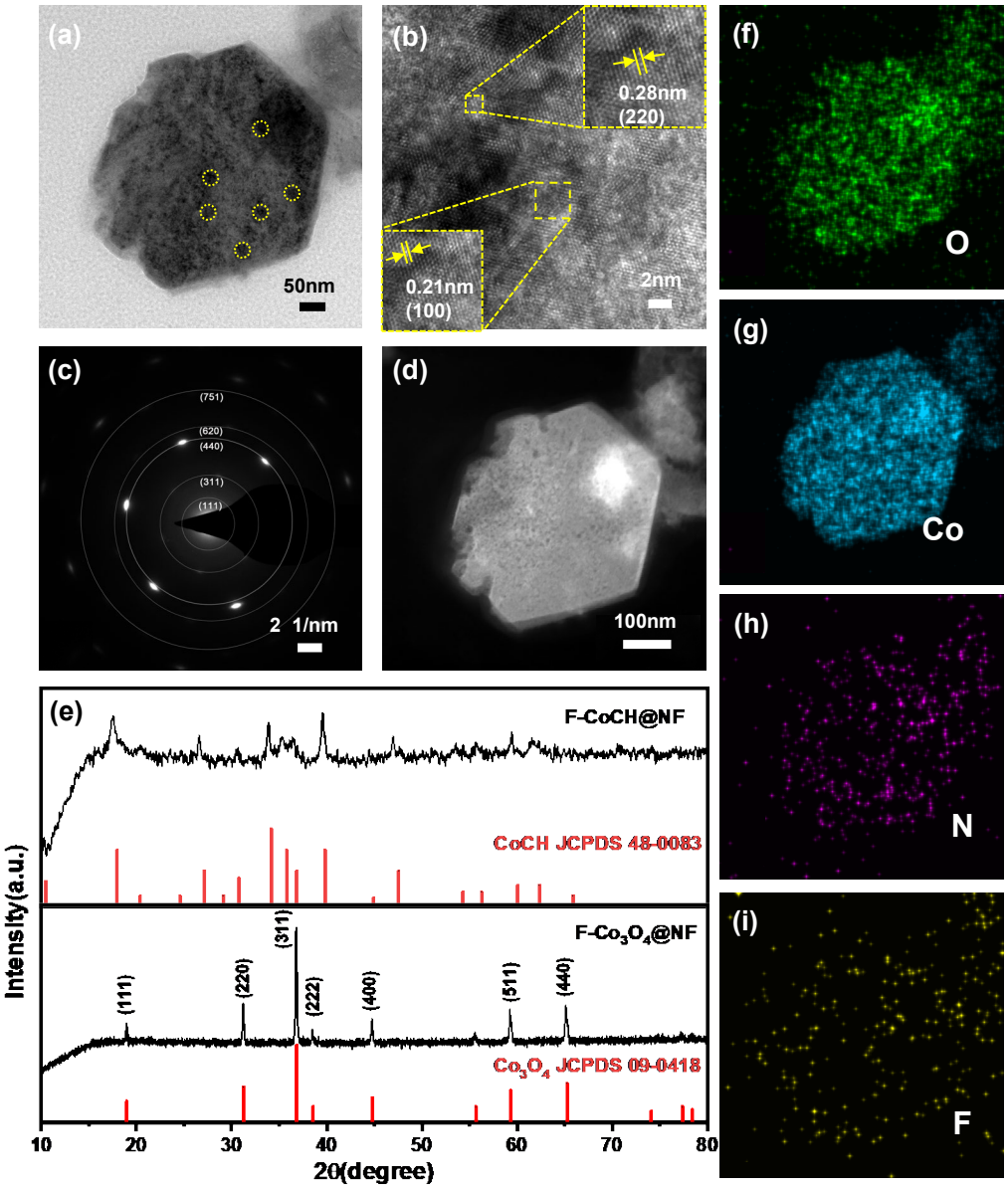

Figure 1 a, b) TEM images of F-Co_3O_4@NF at different magnifications; c) Selected area electron diffraction pattern of F-Co_3O_4@NF; d) HAADF-STEM diagram of F-Co_3O_4@NF; e) XRD spectra of F-CoCH@NF and F-Co_3O_4@NF composites; f-i) the element mapping graph corresponding

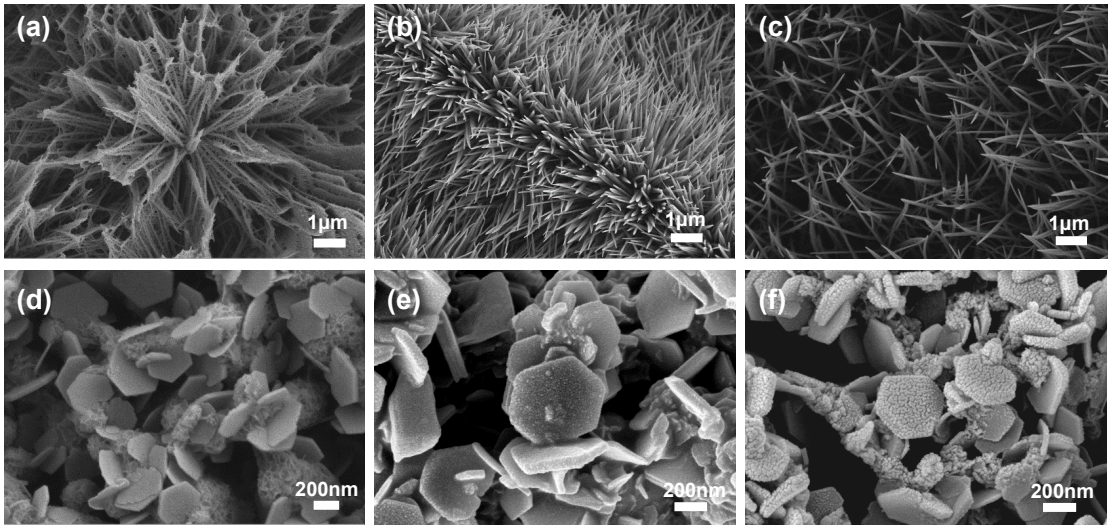

Figure 2 SEM images of a) CoCH@NF; b) F-CoCH@NF; c) Cl-CoCH@NF; d) Co_3O_4@NF; e) F-Co_3O_4@NF; f) Cl-Co_3O_4@NF

The chemical state of each element in the composite catalyst were analyzed using X-ray photoelectron spectroscopy (XPS), as shown in Figure 3. The high-resolution XPS spectra of Co 2p (Fig. 3a) can be divided into three groups of peaks. The peaks at 779.6 eV ($2p_{3/2}$) and 794.6 eV ($2p_{1/2}$) are ascribed to the characteristic peaks of Co^{3+}, and the peaks at 780.6 eV ($2p_{3/2}$) and 796 eV ($2p_{1/2}$) are ascribed to the characteristic peaks of Co^{2+}. The peaks at 788.1 eV and 803.8 eV correspond to the satellite peaks of Co. These results are consistent with the previous reports for Co_3O_4[15] . In addition, the peak area of Co^{3+} corresponding to Co_3O_4@NF catalyst was significantly lower than that of F-Co_3O_4@NF and Cl-Co_3O_4@NF catalysts, indicating that halogen promoted the transition between Co^{2+} and Co^{3+}. This is because F has a strong electronegativity, which may absorb an electron from the Co atom, thereby reducing the electron density around Co[9]. The exposure of high concentration of Co^{3+} is beneficial to the charge transfer in the electrochemical process and improves the electrocatalytic performance[27]. The high-resolution C 1s spectrum of Co_3O_4/C@NF (Figure 3b) revealed three deconvolution peaks at 284, 285.7 and 288.4 eV, corresponding to C-C, C-N and O-C=O bonds, respectively. The C-C, C-N, and O-C=O peaks were also found in the F-Co_3O_4/C@NF and Cl-Co_3O_4/C@NF samples, suggesting that the fundamental structural unit of the C substrate remained unchanged. We also observed a negative shift in the binding energy corresponding to the C-N bond, which may be due to the electron

transfer from Co to N[18]. The peaks observed at 291.9 eV and 294.7 eV in the Cl-Co_3O_4/C@NF material are attributed to the CCl_2 and CCl_3 bonds, respectively. In the F-Co_3O_4/C@NF material, the peaks observed at 291.7 eV and 294.5 eV correspond to the CF_2 and CF_3 bonds[29] , respectively. The C-F bond is covalent or semi-ionic, which is easy to form at the defects of the carbon structure or the oxygen-containing functional groups at the carbon edge[30]. It is worth noting that the C-F bond possesses a polar dipole moment due to the significant difference in electronegativity between F and C, thereby enhancing the electron/ion transfer rate [30].The N 1s spectrum show that the N doped in the carbon support have three forms (pyridine nitrogen, pyrrole nitrogen, graphite nitrogen), but mainly in the form of pyrrole nitrogen. The N 1s spectrum (Figure S4) proves that the N present in the carbon support exists in three different forms, namely pyridine nitrogen, pyrrole nitrogen, and graphite nitrogen. However, the predominant form is that of pyrrole nitrogen. The O 1s spectrum of F-Co_3O_4@NF sample (Figure 3c) shows two peaks centered at 529.8 eV and 531.2 eV, which are attributed to Co-O bond and C-O bond, respectively, indicating the formation of cobalt oxide. The Co-O bond moves to the direction of high binding energy, indicating that the electron density around Co and O decreases, which is likely to flow to F atoms. Compared with the Co_3O_4@NF sample (529.5 eV), the displacement of F-Co_3O_4@NF is 0.2 eV more than that of Cl-Co_3O_4@NF, which could be the reason for the stronger electronegativity of F.

The single peak at 689.3 eV is the fine structure spectrum of F 1s[9, 30]. The single peak at 197.5 eV and 199.3 eV is the fine structure spectrum of Cl 2p (Figure 3d). Recent studies have indicated that incorporating highly electronegative ions into catalysts can modulate their electronic structure, ultimately enhancing their electrocatalytic activity. [7, 8, 31, 32]. The above XPS spectra show that the basic structure of C-C connected carbon-based materials is formed during the hydrothermal process of C-containing raw materials, and the successful doping of F ions is derived from ammonium fluoride. The strong electronegativity of F ions causes the electronic structure of Co_3O_4 to change and the proportion of Co^{3+} to increase.

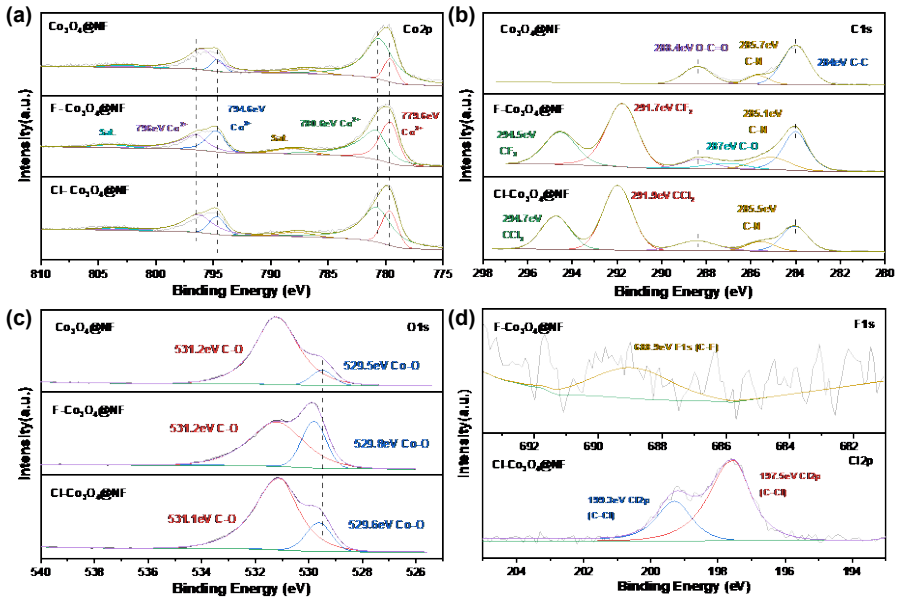

Figure 3 High-resolution XPS spectra of the composites: a) Co 2p; b) C 1s; c) P 2p; d) F 1s and Cl 2p

2.2 Electrocatalytic oxygen evolution properties of composites

We utilized a standard three-electrode system to evaluate the electrocatalytic OER performance of the F-Co_3O_4@NF, Cl-Co_3O_4@NF, Co_3O_4@NF, and bare NF catalysts in 1 M KOH electrolyte. The linear sweep voltammetry (LSV) of all samples at room temperature was examined at a scan rate of 5 mV s^{-1} as demonstrated in Figure 4a. It was noted that the F-Co_3O_4@NF composite catalyst exhibited superior OER activity, as evidenced by its significantly lower overpotential of 42 mV at a current density of 10 mA cm^{-2}, as compared to the Cl-Co_3O_4@NF, bare NF, and Co_3O_4@NF catalysts, which required overpotentials of 146 mV, 248 mV, and 275 mV, respectively. Importantly, the overpotential of F-Co_3O_4@NF in our work was lower than many catalysts reported in similar systems, as shown in Figure 4b.[3, 8, 15, 17, 28, 33-35] Even at a high current density of 50 mA cm^{-2}, the F-Co_3O_4@NF catalyst requires an overpotential of only 172 mV. These results highlight that the doping of halogen, especially F element, exerts a beneficial influence on the catalyst's activity.

The Tafel slope of the F-Co_3O_4@NF composite catalyst (shown in Fig. 4b) is 88 mV dec^{-1}, which is smaller than that of the Cl-Co_3O_4@NF (95 mV dec^{-1}), bare NF (188

mV dec^{-1}), and Co_3O_4@NF (265 mV dec^{-1}). This indicates that the F-Co_3O_4@NF catalyst has a stronger OER catalytic kinetics.

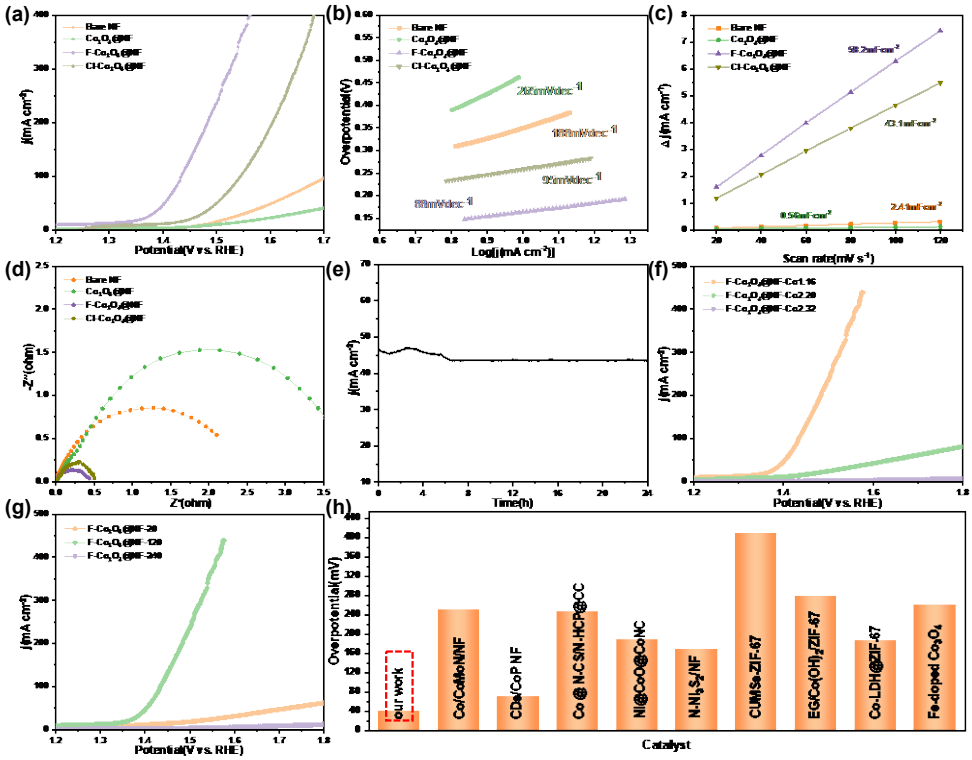

Figure 4 OER characterization of bare NF, Co_3O_4@NF, F-Co_3O_4@NF, Cl-Co_3O_4@NF composite catalysts in 1 M KOH: a) OER polarization curve; b) Tafel slope; c) C_{dl} value; d) EIS spectrum; e) The current density-time curve of F-Co_3O_4@NF; f) OER polarization curves of F-Co_3O_4@NF based on catalyst materials with different impregnation time; g) OER polarization curve of F-Co_3O_4@NF catalyst material based on Co feed amount change; h) Comparison of catalytic performance of similar system catalysts[3, 8, 15, 17, 28, 33-35](overpotential at current density of 10 mA cm^{-2})

Additionally, cyclic voltammetry curves were recorded at different scan rates (20, 40, 60, 80, 100, 120 mV s^{-1}, shown in Figure S2) and used to plot an electrical double-layer capacitor. The slope of the straight line obtained from this plot (shown in Fig. 4c) was used to determine the double layer capacitance C_{dl}. Previous research has shown that the electric double layer capacitance is proportional to the active specific surface area (ECSA) of the catalyst. The F-Co_3O_4@NF catalyst has the largest C_{dl} value of 58.2 mF cm^{-2} in 1 M KOH solution, indicating it has the largest ECSA and can effectively

increase the number of active sites, thus exhibiting the best OER catalytic activity.

The electrochemical impedance spectroscopy (EIS) spectrum (Figure 4d) indicates that the F-Co_3O_4@NF catalyst exhibits the smallest arc radius, which suggests that it has the lowest charge transfer resistance and the highest electron transfer efficiency during catalytic reactions.

The stability analysis of the F-Co_3O_4@NF catalyst was further assessed through a 24-hour chronoamperometry experiment (Figure 4e). Results indicated that in the first 6 hours, there was a slight decrease in the current density. However, for the remaining 18 hours, there was no significant change in the current density, thereby proving the high stability of the catalyst. Furthermore, a consistent catalytic performance of approximately 94% was maintained by the F-Co_3O_4@NF catalyst.

2.3 First-principles calculation

In order to evaluate the catalytic performance of OER, we calculated the Gibbs free energy of each step and used DFT to explore the relationship between electronic structure and intrinsic activity. In an alkaline electrolyte, the electrocatalyst adsorbs water molecules on its surface and then dissociates to catalyze the reaction. Therefore, the energy evolution during water splitting is an important indicator of electrocatalytic performance. OER in alkaline electrolytes requires four electron-proton transfer processes. Figure 5a shows the alkaline OER reaction pathway of F-Co_3O_4@NF catalyst in the standard potential range of 1.23 V. We used the reaction of *O to *OOH as the potential measurement step (PDS). F-Co_3O_4@NF has a lower energy barrier (0.68 eV) than Cl-Co_3O_4@NF (0.75 eV) and Co_3O_4@NF (1.34 eV). The calculated results are in good agreement with the experimental observations. F-Co_3O_4@NF promotes the decomposition of water and reduces the thermodynamic energy barrier of electrolytic oxygen production. The optimized structure of each step in OER is shown in Figure 5b. Figure 5c shows the surface charge density difference of F-Co_3O_4@NF, indicating that the electron of Co_3O_4 transfers to halogen under the influence of the electronegativity of F. The density of states (DOS) confirmed the modulation of the electronic structure of Co_3O_4 by doping halogen ions (Figure 5d). The d-band center was shifted from Co_3O_4@NF (-1.8) to X-Co_3O_4@NF (-1.4) (X = F, Cl). The d-band

center theory shows that the more positive the d-band center is, the closer it is to the Fermi level, which will lead to a stronger binding between the adsorbate and the catalyst surface, which means that the adsorption of X-Co_3O_4@NF (X = F, Cl) oxygen-containing intermediates on the catalyst surface is stronger than that of Co_3O_4 @ NF. The energetic difference at a potential of U = 0 V is shown (Figure S5, Supporting Information). Optimized models of Co_3O_4@NF and Cl-Co_3O_4@NF are shown in Figures S6-S7, Supporting Information. The charge density difference calculation of Cl-Co_3O_4@NF is shown in Figure S8, Supporting Information. Overall, the F-modified Co_3O_4@NF surface showed excellent OER activities.

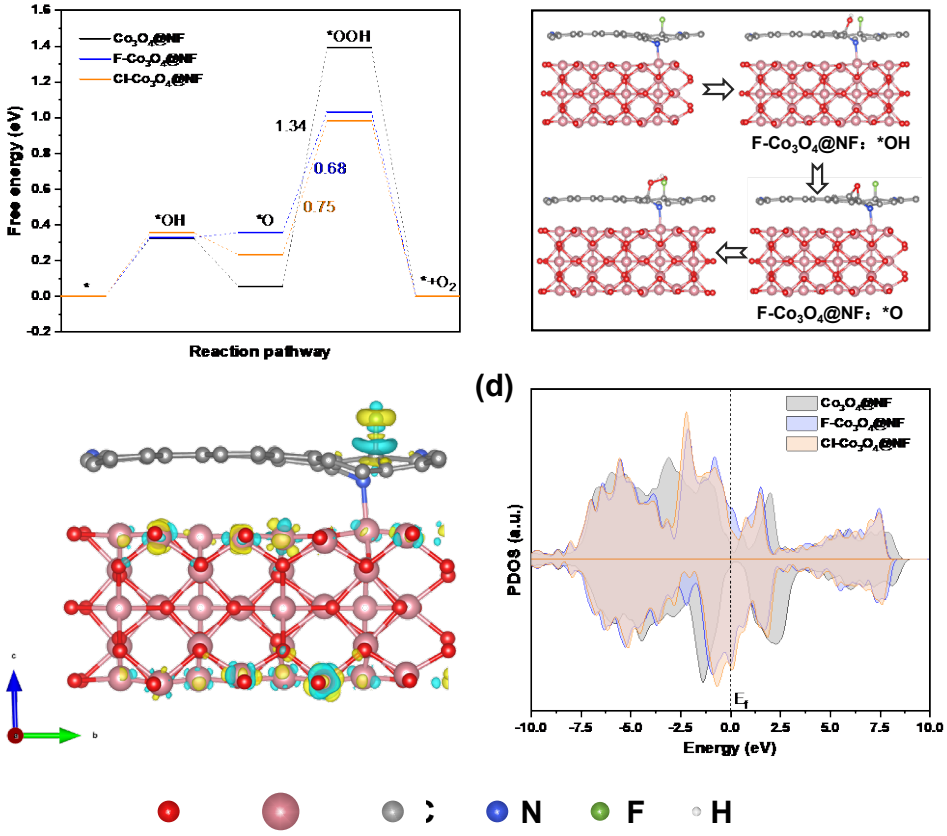

Figure 5. DFT calculation: a) when U = 1.23 V, OER path free energy calculation on the surface of X-Co_3O_4@NF (X = halogen-free, F and Cl) catalyst; b) The initial structure and adsorption structure of the optimized F-Co_3O_4@NF catalyst OER path; c) Surface charge density difference calculation of F-Co_3O_4@NF; d) The density of states of X-Co_3O_4@NF (X = halogen-free, F and Cl) catalysts.

3 Conclusion

In summary, we have confirmed that F anion doping can effectively improve the OER activity of Co_3O_4 by modulating its electronic structure. The prepared F-Co_3O_4@NF catalyst is used for OER catalytic reaction under alkaline conditions. The current density of 50 mA cm^{-2} only requires an overpotential of 172 mV, and the Tafel slope is 88 mV dec^{-1}. Stable catalytic activity can be maintained for 24 h. In addition, we disclose that the incorporation of substantial F atoms will result in upshift the d band center, which are beneficial for the adsorption of intermediates by the catalyst. This method provides a new direction for the design and synthesis of efficient and stable catalysts for OER.

Acknowledgements

This work was financially supported by the National Natural Science Foundation of China (No. U21A20329). The authors express thanks to the Advanced Analysis and Gene Sequencing Center of Zhengzhou University for their support in materials characterization.

Conflict of Interest

The authors declare no conflict of interest.

References

[1] X. Wang, Z. Ma, L. Chai, et al. MOF derived N-doped carbon coated CoP particle/carbon nanotube composite for efficient oxygen evolution reaction[J]. Carbon, 2019, 141: 643-651.

[2] B. You, N. Jiang, M. Sheng, et al. High-performance overall water splitting electrocatalysts derived from cobalt-based metal-organic frameworks[J]. Chemistry of Materials, 2015, 27(22): 7636-7642.

[3] H. Song, J. Yu, Z. Tang, et al. Halogen-doped carbon dots on amorphous cobalt

phosphide as robust electrocatalysts for overall water splitting[J]. Advanced Energy Materials, 2022, 12(14): 2102573.

[4] J. Li, T. Hu, C. Wang, et al. Surface-mediated iron on porous cobalt oxide with high energy state for efficient water oxidation electrocatalysis[J]. Green Energy & Environment, 2022, 7(4): 662-671.

[5] Z. Wang, H. Liu, R. Ge, et al. Phosphorus-Doped Co_3O_4 Nanowire Array: A Highly Efficient Bifunctional Electrocatalyst for Overall Water Splitting[J]. ACS Catalysis, 2018, 8(3): 2236-2241.

[6] L. Xu, Z. Wang, J. Wang, et al. N-doped nanoporous Co_3O_4 nanosheets with oxygen vacancies as oxygen evolving electrocatalysts[J]. Nanotechnology, 2017, 28(16): 165402.

[7] Y. Wu, X. Liu, D. Han, et al. Electron density modulation of $NiCo_2S_4$ nanowires by nitrogen incorporation for highly efficient hydrogen evolution catalysis[J]. Nature Communications, 2018, 9(1): 1425.

[8] T. Kou, T. Smart, B. Yao, et al. Theoretical and experimental insight into the effect of nitrogen doping on hydrogen evolution activity of Ni_3S_2 in alkaline medium[J]. Advanced Energy Materials, 2018, 8(19): 1703538.

[9] W. He, L. Han, Q. Hao, et al. Fluorine-anion-modulated electron structure of nickel sulfide nanosheet arrays for alkaline hydrogen evolution[J]. ACS Energy Letters, 2019, 4(12): 2905-2912.

[10] H.S. Jadhav, H.A. Bandal, S. Ramakrishna, et al. Critical review, recent updates on zeolitic imidazolate framework-67 (ZIF-67) and its derivatives for electrochemical water splitting[J]. Advanced Materials, 2022, 34(11): 2107072.

[11] T. Shi, S. Hussain, C. Ge, et al. ZIF-X (8,67) based nanostructures for gas-sensing applications[J]. Reviews in Chemical Engineering, 2022.

[12] L. Xiao, S. Zheng, K. Yang, et al. The construction of CoP nanoparticles coated with carbon layers derived from core-shell bimetallic MOF for electrochemical detection of dopamine[J]. Microchemical Journal, 2021, 168: 106432.

[13] B. Weng, W. Wei, H. Wu, et al. Bifunctional CoP and CoN porous nanocatalysts derived from ZIF-67 in situ grown on nanowire photoelectrodes for efficient

photoelectrochemical water splitting and CO_2 reduction[J]. Journal of Materials Chemistry A, 2016, 4(40): 15353-15360.

[14] X. Li, Q. Jiang, S. Dou, et al. ZIF-67-derived Co-NC@CoP-NC nanopolyhedra as an efficient bifunctional oxygen electrocatalyst[J]. Journal of Materials Chemistry A, 2016, 4(41): 15836-15840.

[15] Z. Chen, Y. Ha, H. Jia, et al. Oriented transformation of Co-LDH into 2D/3D ZIF-67 to achieve Co-N-C hybrids for efficient overall water splitting[J]. Advanced Energy Materials, 2019, 9(19): 1803918.

[16] Y. Pan, K. Sun, S. Liu, et al. Core-shell ZIF-8@ZIF-67-derived CoP nanoparticle-embedded N-doped carbon nanotube hollow polyhedron for efficient overall water splitting[J]. Journal of the American Chemical Society, 2018, 140(7): 2610-2618.

[17] G. Cai, W. Zhang, L. Jiao, et al. Template-directed growth of well-aligned MOF arrays and derived self-supporting electrodes for water splitting[J]. Chemical Communications, 2017, 2(6): 791-802.

[18] X. Huang, X. Xu, C. Li, et al. Vertical CoP nanoarray wrapped by N, P-doped carbon for hydrogen evolution reaction in both acidic and alkaline conditions[J]. Advanced Energy Materials, 2019, 9(22): 1803970.

[19] Y. Li, S. Niu, D. Rakov, et al. Metal organic framework-derived CoPS/N-doped carbon for efficient electrocatalytic hydrogen evolution[J]. Nanoscale, 2018, 10(15): 7291-7297.

[20] L. Chai, Z. Hu, X. Wang, et al. Stringing bimetallic metal-organic framework-derived cobalt phosphide composite for high-efficiency overall water splitting[J]. Advanced Science, 2020, 7(5): 1903195.

[21] Q. Zhou, B. Jin, P. Zhao, et al. rGO/CNQDs/ZIF-67 composite aerogel for efficient extraction of uranium in wastewater[J]. Chemical Engineering Journal, 2021, 419: 129622.

[22] F. Guo, Y. He, H. Zeng, et al. Surface engineering of ZIF-L renders multidoped leaf-like porous carbon nanosheets for highly efficient oxygen reduction reaction in both alkaline and acidic media[J]. Colloids and Surfaces A: Physicochemical and Engineering Aspects, 2022, 648: 129417.

[23] F. Zhang, L. Chen, H. Yang, et al. Ultrafine Co nanoislands grafted on tailored interpenetrating N-doped carbon nanoleaves: An efficient bifunctional electrocatalyst for rechargeable Zn-air batteries[J]. Chemical Engineering Journal, 2022, 431: 133734.

[24] X. Sang, H. Wu, N. Zang, et al. Co_2P nanoparticle/multi-doped porous carbon nanosheets for the oxygen evolution reaction[J]. New Journal of Chemistry, 2021, 45(19): 8769-8774.

[25] A. Qd, A. Lg, A. Dw, et al. Metal-organic framework derived Co_3O_4/TiO_2 heterostructure nanoarrays for promote photoelectrochemical water splitting[J]. International Journal of Hydrogen Energy, 2021, 46(49): 24965-24976.

[26] Y. Guan, Y. Li, S. Luo, et al. Rational design of positive-hexagon-shaped two-dimensional ZIF-derived materials as improved bifunctional oxygen electrocatalysts for use as long-lasting rechargeable Zn-Air batteries[J]. Applied Catalysis B: Environmental, 2019, 256: 117871.

[27] L.-C. Zhang, H. Chen, G.-R. Hou, et al. Puzzle-inspired carbon dots coupled with cobalt phosphide for constructing a highly-effective overall water splitting interface[J]. Chemical Communications, 2020, 56(2): 257-260.

[28] H. Ma, Z. Chen, Z. Wang, et al. Interface Engineering of Co/CoMoN/NF Heterostructures for High-Performance Electrochemical Overall Water Splitting[J]. Advanced Science, 2022, 9(11): 2105313.

[29] Y. Hu, L. Zhang, P. Zhao, et al. Ultrasensitive luteolin electrochemical sensor based on zeolitic imidazolate frameworks-derived cobalt trioxide@nitrogen doped carbon nanotube/amino-functionalized graphene quantum dots composites modified glass carbon electrode[J]. Sensors and Actuators: B. Chemical, 2022, 351: 130938.

[30] D.-Y. Shin, K.-W. Sung, H.-J. Ahn. Fluorine-doped carbon quantum dot interfacial layer on stockade-like etched copper foil for boosting Li-ion storage[J]. Chemical Engineering Journal, 2021, 413: 127563.

[31] J. Hu, C. Zhang, X. Meng, et al. Hydrogen evolution electrocatalysis with binary-nonmetal transition metal compounds[J]. Journal of Materials Chemistry A, 2017,

5(13): 5995-6012.

[32] P. Chen, T. Zhou, M. Zhang, et al. 3D nitrogen-anion-decorated nickel sulfides for highly efficient overall water splitting[J]. Advanced Materials, 2017, 29(30): 1701584.

[33] J. Cao, C. Lei, J. Yang, et al. An ultrathin cobalt-based zeolitic imidazolate framework nanosheet array with a strong synergistic effect towards the efficient oxygen evolution reaction[J]. Journal of Materials Chemistry A, 2018, 6(39): 18877-18883.

[34] Z. Li, X. Zhang, Y. Kang, et al. Interface engineering of Co-LDH@MOF heterojunction in highly stable and efficient oxygen evolution reaction[J]. Advanced Science, 2021, 8(2): 2002631.

[35] S.L. Zhang, B.Y. Guan, X.F. Lu, et al. Metal atom-doped Co_3O_4 hierarchical nanoplates for electrocatalytic oxygen evolution[J]. Advanced Materials, 2020, 32(31): 2002235.